

**NOAA NESDIS
CENTER for SATELLITE APPLICATIONS and
RESEARCH**

ABI Ozone Detection

ALGORITHM THEORETICAL BASIS DOCUMENT

NOAA/NESDIS/STAR

Version 2.0

September 30, 2010

TABLE OF CONTENTS

	<u>Page</u>
LIST OF FIGURES.....	4
LIST OF TABLES.....	5
LIST OF ACRONYMS.....	6
ABSTRACT.....	7
1. INTRODUCTION.....	8
1.1 Purpose of This Document.....	8
1.2 Who Should Use This Document.....	8
1.3 Inside Each Section.....	8
1.4 Related Documents.....	9
1.5 Revision History.....	9
2. OBSERVING SYSTEM OVERVIEW.....	11
2.1 Products Generated.....	11
2.2 Instrument Characteristics.....	11
3. ALGORITHM DESCRIPTION.....	13
3.1 Algorithm Overview.....	14
3.2 Processing Outline.....	14
3.3 Algorithm Input.....	15
3.3.1 Primary Sensor Data.....	16
3.3.2 Ancillary Data.....	16
3.3.3 Derived Sensor Data.....	17
3.4 Theoretical Description.....	17
3.4.1 Physics of the Problem.....	18
3.4.2 Mathematical Description.....	19
3.4.2.1 Generating Regression Coefficients.....	19
3.4.2.2 Calculating Ozone With Regression.....	20
3.4.2.3 Basic Assumptions in Using Regression for Ozone.....	21
3.4.2.4 Ozone Detection Decision Tree.....	22
3.4.2.5 Input ABI, NWP data, and other predictors.....	22
3.4.2.6 Configure angles, load predictors.....	22
3.4.2.7 Test total column ozone against thresholds.....	22
3.4.3 Algorithm Output.....	22
4. TEST DATASETS AND OUTPUTS.....	24
4.1 Simulated Input Data Sets.....	24
4.2 Output from Simulated Inputs Data Sets.....	27
4.2.1 Precision and Accuracy Estimates.....	27
4.2.2 Error Budget.....	30
5. PRACTICAL CONSIDERATIONS.....	36
5.1 Numerical Computation Considerations.....	37

5.2	Programming and Procedural Considerations	37
5.3	Quality Assessment and Diagnostics	37
5.4	Exception Handling	37
5.5	Algorithm Validation	38
6.	ASSUMPTIONS AND LIMITATIONS	38
6.1	Performance	38
6.2	Assumed Sensor Performance	38
6.3	Pre-Planned Product Improvement.....	39
6.3.1	Increased number of training profiles.....	39
6.3.2	Ozone over low clouds.....	39
6.3.3	Missing inputs	39
7.	REFERENCES.....	39
	APPENDIX 1: COMMON ANCILLARY DATA SETS.....	42
1.	LAND_MASK_NASA_1KM.....	42
a.	<i>Data description</i>	42
b.	<i>Interpolation description</i>	42
2.	NWP_GFS.....	42
a.	<i>Data description</i>	42
b.	<i>Interpolation description</i>	42

LIST OF FIGURES

	<u>Page</u>
Figure 3.1 High level flowchart of the ABI Ozone code illustrating the main processing sections.....	15
Figure 3.2 Atmospheric weighting functions for SEVIRI, ABI, and the current GOES Sounder. SEVIRI and ABI are very similar, where as the GOES Sounder has higher sensitivity in the upper atmosphere.....	18
Figure 3.3 Locations of the profiles used in the training dataset.....	20
Figure 4.1 SEVIRI TCO data for 23 UTC on 1 August 2006. The red fringe is due to the visualization software.....	26
Figure 4.2 SEVIRI TCO at 1:00 UTC and 12:00 UTC on 1 August 2006. Left: 1:00 UTC 1 August 2006, Right: 12:00 UTC 1 August 2006.....	27
Figure 4.3 Met-8 SEVIRI total column ozone co-located in time and space with OMI total column ozone. Only SEVIRI clear-sky pixels were used.....	29
Figure 4.4 OMI total column ozone for 14-15 February 2007. Locations corresponding to SEVIRI clear-sky pixels were used.....	30
Figure 4.5. Met-8 SEVIRI vs OMI total column ozone for all cloud-free pixels during the test data period August 2006, February 1-14 and April 1-10 2007. Accuracy is 3.3 DU and precision is 14.8 DU.....	33
Figure 4.6. Met-8 SEVIRI vs OMI total column ozone for all cloud-free, non-desert land pixels during the test data period August 2006, February 1-14 and April 1-10 2007. Accuracy is 3.3 DU and precision is 14.4 DU.....	34
Figure 4.7. Met-8 SEVIRI vs OMI total column ozone for all cloud-free desert pixels during the test data period August 2006, February 1-14 and April 1-10 2007. The high ozone bias of Met-8 total column ozone over desert can be seen as the large region of points above the 1:1 line. Accuracy is 14.8 DU and precision is 12.9 DU.....	35
Figure 4.8. Met-8 SEVIRI vs OMI total column ozone for all cloud-free pixels during the test data period August 2006, February 1-14 and April 1-10 2007. Accuracy is 1.5 DU and precision is 13.1 DU.....	36

LIST OF TABLES

	<u>Page</u>
ABI Ozone Detection Algorithm Theoretical Basis Document Version History Summary	9
Table 2.1 GOES-R mission requirements for ozone detection	11
Table 2.2 Spectral characteristics of Advanced Baseline Imager	13
Table 3.1 Input list of required sensor data.....	16
Table 3.2 Input list of required non-ABI ancillary dynamic data	17
Table 3.3 Input list of required non-ABI ancillary static data	17
Table 3.4 Input list of derived sensor data	17
Table 3.5 Explanation of terms for generating regression	19
Table 3.6 Explanation of terms for solving regression	20
Table 3.7 Expanded terms of regression equation	21
Table 3.8 Summary of ABI ozone code output data	23
Table 4.1 Bands used for ozone regression with different instruments.....	25
Table 4.2 Comparison of SEVIRI and OMI Validation to Requirements	28
Table 4.3 Accuracy and Precision Results for Met-8 SEVIRI vs OMI Comparisons	31

LIST OF ACRONYMS

ADEB	Algorithm Development Executive Board
AIT	Algorithm Integration Team
ATBD	Algorithm Theoretical Base Document
AWG	Algorithm Working Group
CDR	Critical Design Review
CICS	Cooperative Institute for Climate Studies
CIMSS	Cooperative Institute for Meteorological Satellite Studies
CM	Configuration Management
CMMI	Capability Maturity Model Integration
CREST	Cooperative Remote Sensing and Technology Center
DG	Document Guideline
EPL	Enterprise Product Lifecycle
GOES	Geostationary Operational Environmental Satellite
GS-F&PS	Ground Segment Functional and Performance Specification
IPR	Independent Peer Review
IPT	Integrated Product Team
NESDIS	National Environmental Satellite, Data, and Information Service
NOAA	National Oceanic and Atmospheric Administration
MRD	Mission Requirement Document
OCD	Operations Concept Document
OMI	Ozone Monitoring Instrument
PDR	Preliminary Design Review
PRR	Project Requirements Review
QA	Quality Assurance
RAD	Requirements Allocation Document
RAS	Requirements Allocation Sheet
RMSE	Root Mean Square Error
RNM	Requirements/Needs Matrix
RPP	Research Project Plan
SPSRB	Satellite Products and Services Review Board
SRR	System Readiness Review
STAR	Center for Satellite Applications and Research
SWA	Software Architecture Document
TCO	Total Column Ozone
TD	Training Document
TOMS	Total Ozone Mapping Spectrometer
VVP	Verification and Validation Plan

ABSTRACT

Since 1998 data from the GOES I-M Sounders has been used to generate ozone on an hourly basis. In spite of the relatively coarse spatial and temporal resolution of the current GOES Sounder (8 km spaced every 10 km at nadir, hourly CONUS data) the algorithm has shown that geostationary infrared data can be used to monitor total column ozone. The data has been applied to studies of atmospheric dynamics, reflecting the relationship between ozone and potential vorticity in the stratosphere, and air quality, primarily as a source function in air quality and ozone prediction models.

The ABI ozone algorithm is similar to the GOES ozone algorithm. The specific objectives of ABI ozone detection algorithm development are listed below.

- Adapt current GOES Sounder ozone algorithm to GOES-R ABI accounting for the differences in spectral coverage
- Address needs of user community and meet GOES-R ozone product mission requirements.
- Provide smooth transition from current GOES Sounder to the next generation ABI.
- Ensure continuity/consistency of a long-term (1995-GOES-R era) geostationary ozone data base.
- Incorporate flexibility for enhancements as demonstrated with GOES-R research.
- Implementation simplicity and operational robustness.

The current version of the GOES ozone product provides the total column ozone for a given pixel. The air quality user community has requested higher accuracy and the dynamics community wants higher spatial resolution.

1. INTRODUCTION

The purpose, users, scope, related documents and revision history of this document are briefly described in this section. Section 2 gives an overview of the observing system and instrument characteristics, objectives of the ozone detection algorithm development, mission requirements, and retrieval strategies. Section 3 describes the ABI ozone algorithm and processing outline, input data requirements, theoretical and physical description of ozone monitoring, and algorithm output. Test data sets and sample output is presented in Section 4. Practical considerations are presented in Section 5. Assumptions and limitations are outlined in Section 6 and Section 7 provides a list of references.

1.1 Purpose of This Document

The ABI ozone detection algorithm theoretical basis document (ATBD) provides a high level description of diurnal ozone monitoring utilizing the next generation GOES-R series Advanced Baseline Imager (ABI). The purpose of the GOES-R ABI Ozone ATBD is to provide ozone product developers, reviewers and users with a theoretical description (scientific and mathematical) of the algorithm. This document presents an overview of requirements for the ABI ozone product, ABI characteristics pertinent to ozone monitoring, required input data, the physical and mathematical backgrounds of the algorithm, predicted performance based on case study analyses, practical considerations, and assumptions and limitations. Also, this document provides information useful to anyone maintaining or modifying the original algorithm.

1.2 Who Should Use This Document

The intended users of this document are those interested in understanding the physical basis of the ABI ozone algorithm and how to use the output of this algorithm for a variety of ozone applications. This includes a broad user community with various degrees of satellite expertise. The ABI ozone product expands on the current GOES Sounder ozone product which is utilized by various users for air quality applications.

1.3 Inside Each Section

This document is broken down into the following main sections.

- **Observing System Overview:** Provides relevant details of the ABI and provides a brief description of the product generated by the ozone algorithm.
- **Algorithm Description:** Provides a detailed description of the algorithm including its physical basis, its input and its output.
- **Test Data Sets and Output:** Provides a description of the test data sets used to develop and implement the algorithm and characterize the performance of the algorithm.
- **Practical Considerations:** Provides a brief overview of the issues relating to numerical computation, programming and procedures, configuration of retrieval, quality assessment and diagnostics, and exception handling.

- **Assumptions and Limitations:** Provides an overview of the current limitations of the instrument and algorithm and possible avenues for addressing some of these limitations with further algorithm development.

1.4 Related Documents

This document may contain information from other GOES-R documents listed in the website provided by the GOES-R algorithm working group (AWG):
<http://www.orbit2.nesdis.noaa.gov/star/goesr/index.php>.

In particular, readers are directed to read these documents for a good understanding of the goals of this ATBD:

- GOES-R Series Ground Segment Functional and Performance
- GOES-R Series Mission Requirements Document
- GOES-R Land Surface Team Critical Design Review (May 2008)

Other related references are listed in the Reference Section.

1.5 Revision History

Version 0.1 of this document was created by Chris Schmidt (UW Madison SSEC/CIMSS), and its intent was to accompany the delivery of the version 1.0 algorithm to the GOES-R AWG Algorithm Integration Team (AIT).

Version 1.0 and 1.2 of this document was created by Chris Schmidt (UW Madison SSEC/CIMSS). It was reformatted to fit the 80% delivery guidelines.

Version 2.0 α was created by Chris Schmidt (UW Madison/SSEC/CIMSS) and incorporates comments from initial review of the prior version as well as additional results. This version was submitted for ADEB review. It corresponds to the state of the ozone algorithm at its fifth delivery to the AIT in July, 2010.

Version 2.0 was created by Jay Hoffman and Chris Schmidt (UW Madison/SSEC/CIMSS) and incorporates the input from the AIT and Algorithm Development Executive Board (ADEB) Independent Peer Reviewer (IPR).

ABI Ozone Detection Algorithm Theoretical Basis Document Version History Summary

Version	Description	Revised Sections	Date
0.1	New ATBD Document according to NOAA /NESDIS/STAR Document Guideline		8/4/2008
1.0	Updated to fit 80% delivery format	All	6/19/2009
1.1	Updated re: TRR results	4	9/28/2009
2.0 α	100% delivery document for ADEB review	All	7/25/2010
2.0	100% delivery, ADEB/IPR and AIT comments integrated	All	9/20/2010

2. OBSERVING SYSTEM OVERVIEW

This section provides an overview of the ABI ozone algorithm, including the products generated and objectives and characteristics of the ABI instrument as they pertain to the ABI ozone product development and implementation.

2.1 Products Generated

The ozone product is a clear sky, total column value in Dobson Units (DU). The ozone data can be used in studies of atmospheric dynamics, reflecting the relationship between ozone and potential vorticity in the stratosphere, as well as air quality, primarily as a source function in air quality and ozone prediction models.

The ozone detection requirements defined by the mission requirement document (F&PS v2.1, November 23, 2009) are listed in Table 2.1.

Table 2.1 *GOES-R mission requirements for ozone detection*

Ozone requirements for GOES-R mission										
Observational Requirement	Geographic Coverage ¹	Horiz. Res.	Mapping Accuracy	Measurement range (DU)	Precision (DU)	Accuracy (DU)	Refresh Rate	Data Latency	Product Type	Product Sub-Type
Ozone Total	C, FD	10 km	5 km	100-650	25	15	60 min	5 min	Atmosphere	Trace Gases

¹ C=CONUS, FD=full disk, H=hemisphere, M=mesoscale

The product qualifiers are that it is a day and night algorithm, quantitative to 65° LZA and qualitative beyond, and is valid for clear-sky pixels.

This product was originally to be both for the hyperspectral sounder that was once planned for GOES-R and the ABI. While precision and accuracy were adjusted to account for ABI, the refresh rate and horizontal resolution were left at the values for the sounder. The algorithm as developed, however, can meet these requirements at ABI resolution, as illustrated in Section 4.2. Aggregation to 10 km can be accomplished prior to product distribution if necessary.

2.2 Instrument Characteristics

The next generation GOES-R ABI offers the basics needed for infrared ozone detection. The ABI will provide full disk coverage every 15 minutes and CONUS coverage every 5 minutes at 2 km in the short and long-wave infrared window bands. Those characteristics improve the spatial resolution but ABI lacks the bands sensitive to CO₂ emissions in the upper atmosphere, thus reducing overall accuracy relative to the GOES Sounder. Comparable performance can be achieved if temperature profile data from a model is used in the algorithm. The GOES-R ABI ozone product will be complementary to those derived from ultraviolet-based ozone instruments,

providing ozone over the course of the entire day, instead of just near local solar noon when UV instruments typically take their measurements.

For ozone monitoring the ABI's channels are essentially the same spectrally as the channels on Met-8/-9 SEVIRI, making it an excellent test bed for the ABI algorithm. The algorithm is a regression, and it has been shown that the regression extracts basically all of the available ozone information from broadband IR data that includes the ozone sensitive band around 9.6 μm .

Table 2.2 Spectral characteristics of Advanced Baseline Imager

ABI spectral characteristics						
Channel Number	Wavelength (μm)	Bandwidth (μm)	NEDT/SNR	Upper Limit of Dynamic Range	Spatial Resolution	Used in ABI ozone code
1	0.47	0.45 – 0.49	300:1 ^[1]	652 W/m ² /sr/μm	1 km	
2	0.64	0.59 – 0.69	300:1 ^[1]	515 W/m ² /sr/μm	0.5 km	
3	0.86	0.8455 – 0.8845	300:1 ^[1]	305 W/m ² /sr/μm	1 km	
4	1.38	1.3705 – 1.3855	300:1 ^[1]	114 W/m ² /sr/μm	2 km	
5	1.61	1.58 – 1.64	300:1 ^[1]	77 W/m ² /sr/μm	1 km	
6	2.26	2.225 – 2.275	300:1 ^[1]	24 W/m ² /sr/μm	2 km	
7	3.9	3.8 – 4.0	0.1 K ^[2]	400 K	2 km	
8	6.15	5.77 – 6.60	0.1 K ^[2]	300 K	2 km	✓
9	7.0	6.75 – 7.15	0.1 K ^[2]	300 K	2 km	✓
10	7.4	7.24 – 7.44	0.1 K ^[2]	320 K	2 km	✓
11	8.5	8.30 – 8.70	0.1 K ^[2]	330 K	2 km	
12	9.7	9.42 – 9.80	0.1 K ^[2]	300 K	2 km	✓
13	10.35	10.10 – 10.60	0.1 K ^[2]	330 K	2 km	✓
14	11.2	10.80 – 11.60	0.1 K ^[2]	330 K	2 km	✓
15	12.3	11.80 – 12.80	0.1 K ^[2]	330 K	2 km	✓
16	13.3	13.0 – 13.6	0.3 K ^[2]	305 K	2 km	✓

[1]100% albedo, [2]300K scene.

The ABI ozone algorithm performs a regression against the indicated channels. The performance of the ozone algorithm is sensitive to instrument noise and other anomalies (striping, etc.). However the largest impact on product quality is the misidentification of clouds and cases that fall well outside the range for which the regression was trained (most often areas with a very low total column water vapor and highly reflective surfaces).

3. ALGORITHM DESCRIPTION

This section provides a description of the algorithm at the current level of maturity.

3.1 Algorithm Overview

GOES-R ABI ozone detection is an Option 2 component of the GOES-R ABI processing system. The ozone detection algorithm is being developed within the GOES-R AWG Air Quality team as part of the air quality module processing subsystem.

The GOES-R ABI allows for nearly continuous earth observation with an instantaneous ground field of view (IGFOV) at nadir for the visible band and 2 km for the infrared bands. Multi-spectral ABI data will be available every 5 minutes over the continental United States with full disk coverage of the Western Hemisphere every 15 minutes. GOES_R ABI offers frequent total column ozone measurements at 2 km resolution. The GOES-R ABI ozone algorithm builds on the experience with the GOES Sounder total column ozone developed at the University of Wisconsin (UW) Cooperative Institute for Meteorological Satellite Studies (CIMSS) as a collaborative effort between NOAA/NESDIS/STAR and UW-CIMSS personnel. (Schmidt, 2000; Li et al, 2001; Li et al, 2007; Jin et al, 2008)

The ABI ozone algorithm is a regression algorithm that uses most of the mid- and long-wave IR bands, model-provided temperature profiles, and select other information to generate total column ozone. The ozone detection algorithm is based primarily on the sensitivity of the 9.7 μm band to ozone absorption but also the relationship between ozone and potential vorticity (and thus the thermal structure of the atmosphere). Two long-wave IR bands, 6.95 μm and 10.35 μm , are not used in the regression as they are unnecessary and degrade product quality. Ozone can be calculated for any pixel, but the regression is designed to work for cloud-free pixels within a local zenith angle of 80°.

The GOES ABI ozone product will be produced for each ABI image and provides total column ozone for data within a satellite view angle of 80°. The final user output consists of a NetCDF4 ozone product providing pixel by pixel mask of ozone values and a product quality indicator identifying ozone values outside of reasonable bounds.

3.2 Processing Outline

Figure 3.1 contains a flowchart of the GOES-R ABI ozone detection algorithm.

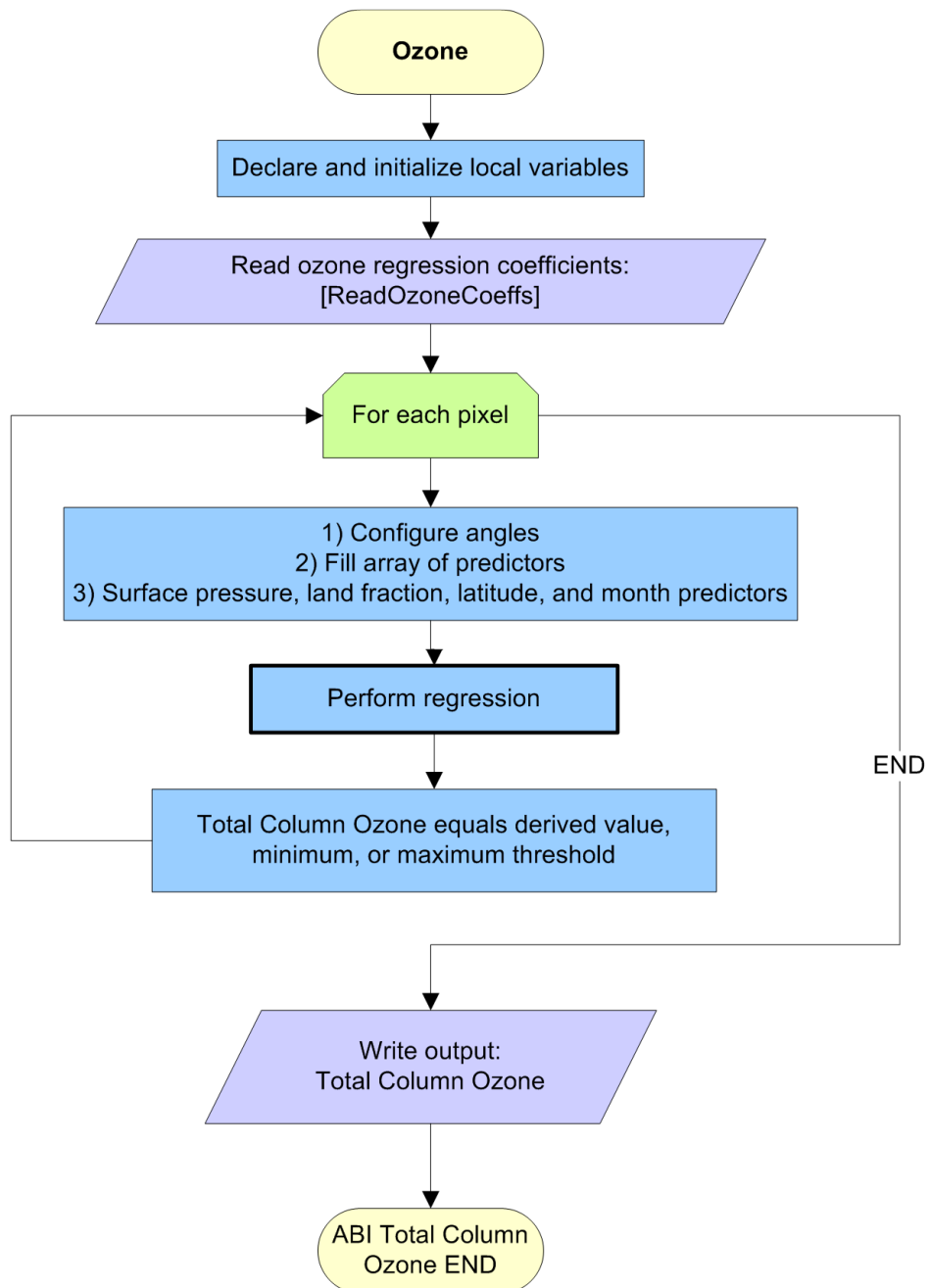


Figure 3.1 High level flowchart of the ABI Ozone code illustrating the main processing sections.

3.3 Algorithm Input

This section describes the input needed to process the GOES-R ABI ozone product. While the ozone code is applied to each pixel it should be used in conjunction with a cloud mask to screen for the cloud-free pixels.

3.3.1 Primary Sensor Data

Table 3.1 lists the primary sensor data used by the ozone code. Primary sensor data means information that is derived solely from the ABI observations and geolocation information. For each pixel the GOES-R ABI ozone algorithm requires calibrated and navigated ABI brightness temperatures/radiances, solar-view geometry (local zenith angle), and ABI sensor quality flags.

Table 3.1 *Input list of required sensor data*

Required sensor data			
Name	Type	Description	Dimension
Ch7 brightness temp/radiances	input	Calibrated ABI level 1b brightness temperatures for channel 7	Scan grid (xsize, ysize)
Ch8 brightness temp/radiances	input	Calibrated ABI level 1b brightness temperatures for channel 8	Scan grid (xsize, ysize)
Ch10 brightness temp/radiances	input	Calibrated ABI level 1b brightness temperatures for channel 10	Scan grid (xsize, ysize)
Ch11 brightness temp/radiances	input	Calibrated ABI level 1b brightness temperatures for channel 11	Scan grid (xsize, ysize)
Ch12 brightness temp/radiances	input	Calibrated ABI level 1b brightness temperatures for channel 12	Scan grid (xsize, ysize)
Ch14 brightness temp/radiances	input	Calibrated ABI level 1b brightness temperatures for channel 14	Scan grid (xsize, ysize)
Ch15 brightness temp/radiances	input	Calibrated ABI level 1b brightness temperatures for channel 15	Scan grid (xsize, ysize)
Ch16 brightness temp/radiances	input	Calibrated ABI level 1b brightness temperatures for channel 16	Scan grid (xsize, ysize)
Solar geometry	input	ABI solar zenith angle	Scan grid (xsize, ysize)
View angles	input	ABI view zenith and relative azimuth angles	Scan grid (xsize, ysize)
QC flags	input	ABI quality control flags with level 1b data	Scan grid (xsize, ysize)

3.3.2 Ancillary Data

The following tables (Tables 3.2 and 3.3) list and briefly describe the non-ABI dynamic and static ancillary data required to run the GOES-R ABI ozone algorithm. By ancillary data, we mean data that requires information not included in the ABI observations or geolocation data. Dynamic ancillary data refers to data sets that change over time, while static ancillary data refers to data sets that remain constant over time.

Table 3.2 *Input list of required non-ABI ancillary dynamic data*

Dynamic non-ABI ancillary data			
Name	Type	Description	Dimension
Temperature profile	input	NCEP NWP temperature profile	0.25° resolution

The NWP data can come from virtually any model that performs well, and the resolution can be coarser though the quality will decrease. The algorithm as designed uses a nearest neighbor match of the pixel to the model data.

Table 3.3 *Input list of required non-ABI ancillary static data*

Static non-ABI ancillary data			
Name	Type	Description	Dimension
Regression coefficients	input	Regression coefficients calculated from training dataset of atmospheric profiles, binned by local zenith angle.	Binned by 1° local zenith angle, 0° to 80°
Land Mask	input	Global 1-km land/water mask used for MODIS collection 5 or comparable substitute.	0.05° resolution

The regression coefficients are generated from a collection of collocated ozone and temperature profiles as described in this document. The land mask can come from any source so long as it is accurate.

3.3.3 Derived Sensor Data

As designed, the ozone algorithm does not directly apply the cloud mask. However, the mask is needed to identify cloud-free pixels. Table 3.4 briefly describes this derived sensor data input.

Table 3.4 *Input list of derived sensor data*

Derived sensor data			
Name	Type	Description	Dimension
Cloud mask	input	ABI level 2 cloud mask data	grid (xsize, ysize)

The cloud mask is the cloud mask created for ABI.

3.4 Theoretical Description

Ozone is present throughout the atmosphere, but the majority of it is above the tropopause in the stratosphere. A substantial amount is present near the tropopause as well. Ozone is strongly correlated to potential vorticity (PV) and by extension temperature in the stratosphere. PV is strongly correlated to tropopause height and by extension the weather we experience at the

surface. By this relationship ozone does vary on the same time scales as weather, specifically synoptic scale weather events but also with mesoscale weather events. In order to detect ozone with a broadband IR instrument, the instrument must have sensitivity to at least one of the following, though both are preferred:

- Stratospheric temperatures
- Ozone absorption (around 9.6 μm)

In GOES Sounder total column ozone studies, published in Li et al (2001), it was found that for regression:

- The ozone band alone could achieve a %RMSE of $\sim 11\%$
- Other bands (Sounder channels 1-8, 10-15) could achieve a %RMSE of $\sim 11\%$
- All Sounder bands together could achieve a %RMSE of $< 5\%$

Those studies showed that the regression is exploiting ozone absorption information and the relationship between stratospheric temperature, potential vorticity, and ozone.

3.4.1 Physics of the Problem

Infrared satellite ozone detection primarily utilizes the 9.6 μm “ozone” band but also makes use of other mid- and long-wave IR bands. IR bands have different detection sensitivities for ozone and temperature at different altitudes. Atmospheric weighting functions (relative band sensitivities) for SEVIRI, ABI, and current generation GOES Sounder are shown in Figure 3.3. It shows that the GOES Sounder has more sensitivity above 200 hPa than SEVIRI and ABI, and that sensitivity is due to bands sensitive to CO_2 emissions. The thermal structure of the atmosphere defines the potential vorticity (PV) of the atmosphere, and PV in the stratosphere is correlated pretty strongly with ozone in the stratosphere, where 90% of the ozone column exists.

ABI does not have as much sensitivity to stratospheric temperature as the GOES Sounder. To make up for the missing information a NWP temperature profile can be used in the regression. (Li et al, 2007; Jin et al, 2008)

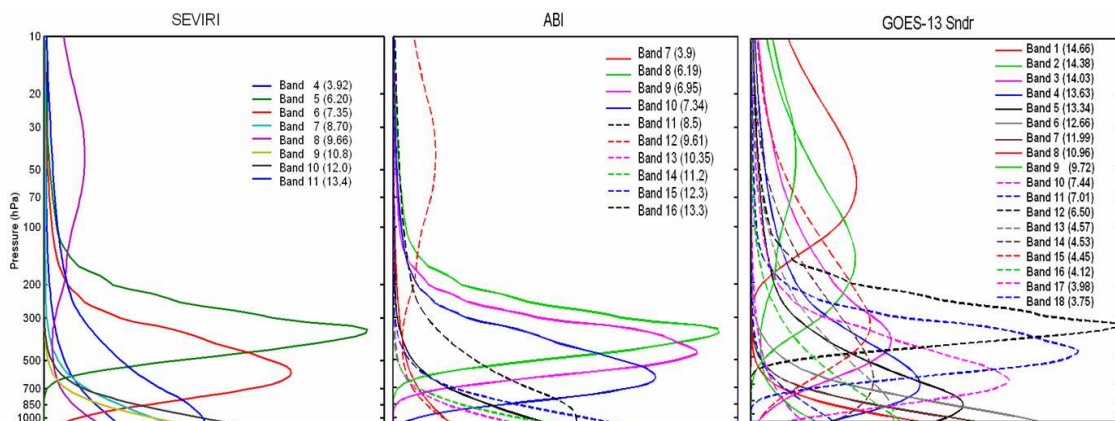


Figure 3.2 Atmospheric weighting functions for SEVIRI, ABI, and the current GOES Sounder. SEVIRI and ABI are very similar, where as the GOES Sounder has higher sensitivity in the upper atmosphere.

3.4.2 Mathematical Description

There are two approaches that can be taken to extract ozone information from the available data: statistical regression and physical retrieval. In studies with the GOES Sounder and initial simulation studies for GOES-R it was shown that the physical retrieval does not achieve better performance than the regression. Regression extracts virtually all of the ozone information from broadband IR radiances. (Schmidt, 2000; Jin et al, 2008)

The ABI ozone regression utilizes the information contained in the ozone band as well as the correlation between ozone and stratospheric temperature to estimate the total column ozone value. The other bands used are listed in Table 2.1. The specific bands chosen for regression vary by instrument, but in general the regression utilizes window channels with minimal water vapor signal. GOES Sounder, simulated ABI, and SEVIRI perform comparably when simulated ABI and SEVIRI regressions are given temperature profiles as predictors to make up for the CO₂ bands on the GOES Sounder. Ozone from IR instruments is generally considered a clear sky product. However future improvements could allow for ozone estimates over some clouds.

3.4.2.1 Generating Regression Coefficients

Regression is the development of a relationship between two sets of data. Curve-fitting is an example. For ozone the regression is finding coefficients that relate total column ozone to a set of values, known as predictors, coming from a training dataset. The generalized form of the equation is shown in Equation 3.1 and the variables explained in Table 3.5.

Table 3.5 Explanation of terms for generating regression

Regression Terms	
C _{NP}	Regression coefficients for NP predictors
O _{NS}	Total column ozone for NS sets of predictors from training dataset
P _{NP,NS}	The training dataset, each location with its data is a column, NS/number of rows is the number of members of the training dataset
NS	Number of members of the training dataset
NP	Number of pieces of information for each member of the training dataset

$$\begin{vmatrix} O_1 \\ \dots \\ \dots \\ O_{NS} \end{vmatrix} = \begin{vmatrix} C_1 & \dots & \dots & C_{NP} \end{vmatrix} \bullet \begin{vmatrix} P_{1,1} & P_{1,2} & \dots & P_{1,NS} \\ P_{2,1} & P_{2,2} & \dots & \dots \\ \dots & \dots & \dots & \dots \\ P_{NP,1} & \dots & \dots & P_{NP,NS} \end{vmatrix} \quad (3.1)$$

To generate the coefficients, >10,000 atmospheric temperature, moisture, and ozone profiles (with associated total column ozone, location, fraction of land at the location, and other

information) located between 70° N and 70° S were selected from a training dataset consisting of NOAA88b profiles, radiosondes, ozonesondes, ECMWF+SBUV data, and TIGR data. A forward model (PFAAST) was used to generate brightness temperatures. Scattering by aerosols was neglected. Local zenith angle is varied for each profile in 0.5° steps from 0° to 80°. The result is 161 sets of coefficients to use to solve for ozone in the regression equation. Figure 3.3 shows the locations of the training dataset profiles. (Schmidt, 2000; Li et al, 2001; Li et al, 2007; Jin et al, 2008)

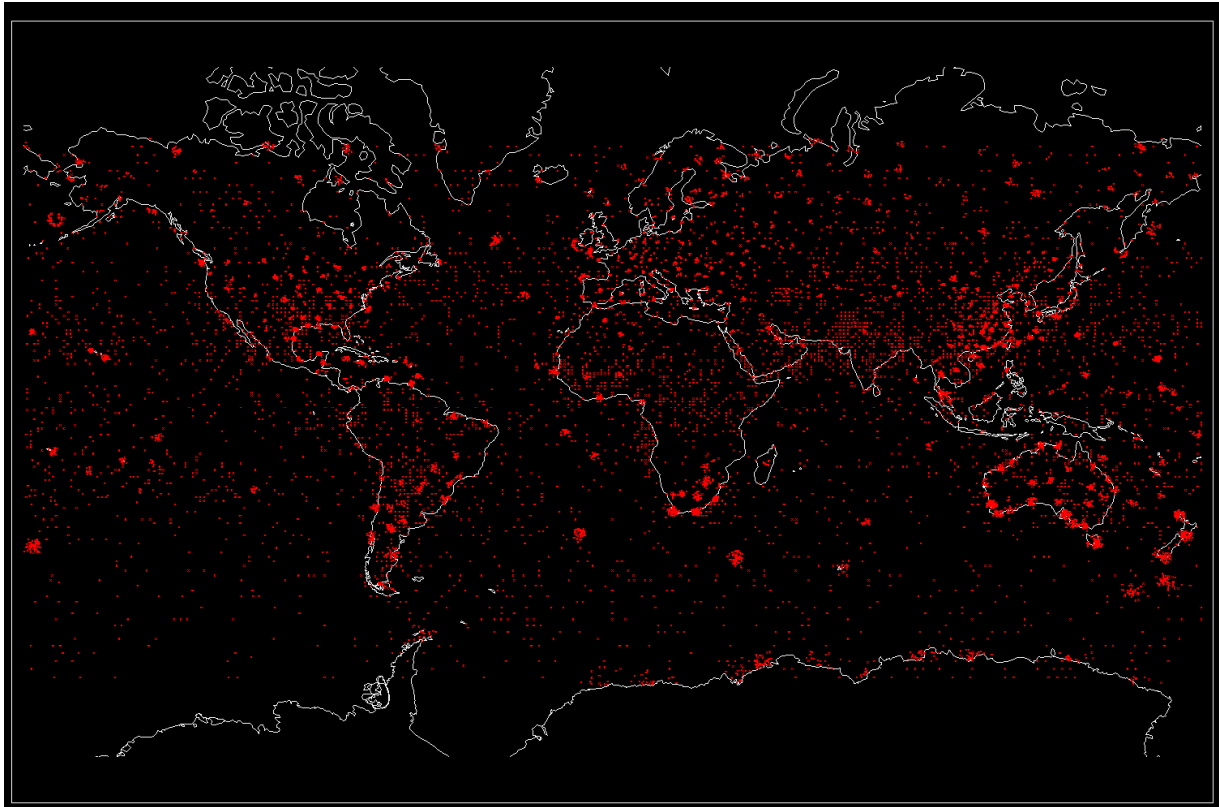


Figure 3.3 *Locations of the profiles used in the training dataset.*

3.4.2.2 Calculating Ozone With Regression

Given the vector \mathbf{C} ozone can be found by calculating the dot product of the coefficients \mathbf{C} and the predictors \mathbf{P} as shown in Equation 3.2. The terms of the equation are listed in Table 3.6.

Table 3.6 *Explanation of terms for solving regression*

Regression Terms	
\mathbf{C}_{NP}	Regression coefficients for NP predictors
O_{TCO}	Total column ozone
\mathbf{P}_{NP}	Predictors (NP of them)
NP	Number of pieces of information for each member of the training dataset

$$O_{\text{TCO}} = \begin{vmatrix} C_1 & \dots & \dots & C_{\text{NP}} \end{vmatrix} \bullet \begin{vmatrix} P_1 \\ \dots \\ \dots \\ P_{\text{NP}} \end{vmatrix} \quad (3.2)$$

The terms are expanded out to the following equation:

$$\ln(\text{TCO}) = C_0 + \sum_{j=1}^n C_j T b_j + \sum_{k=1}^n C_k T b_k^2 + \sum_{l=1}^{101} C_l T a_l + C_{2n+102} p_s + C_{2n+103} L_p + C_{2n+104} \cos\left(\frac{M-6}{12} \pi\right) + C_{2n+105} \cos(\text{LAT}) \quad (3.3)$$

The terms are laid out in Table 3.7.

Table 3.7 Expanded terms of regression equation

Regression Terms	
C_x	Regression coefficients (C_0 is an offset)
n	Number of bands used
Tb	Brightness temperature
Ta	Atmospheric temperature profile
p_s	Surface Pressure
L_p	Fraction of land within pixel
M	Month of year
LAT	Latitude of pixel

Surface pressure is used as a predictor to reduce overall error. Land fraction partially accounts for mixed emissivity but can be just a land vs water flag. The month accounts for a climatological, cyclical variation in ozone. Latitude is also a climatological variable. Each local zenith angle bin has its own coefficients.

3.4.2.3 Basic Assumptions in Using Regression for Ozone

The regression training dataset is assumed to be sufficient for conditions observed by the ABI instrument (based on global and seasonal coverage). There will always be cases not represented by the training dataset which will not perform well with the regression but the training set is big and varied enough to cover the vast majority of circumstances. It is assumed that the pixel is cloud-free and that the input satellite data meets specifications. The NWP temperature profiles are assumed to be at 101 pressure levels, as is standard today.

3.4.2.4 Ozone Detection Decision Tree

The GOES-R ABI ozone algorithm uses a simple approach to determine total column ozone. The needed data is initialized, the regression coefficients are loaded into memory, and for each pixel the regression is performed once the predictors are configured. Figure 3.1 contains the flowchart.

3.4.2.5 Input ABI, NWP data, and other predictors

Required Input ABI data is presented in Section 3.3 of this document. It includes primary sensor data (channels 8-10, 12-16), NWP temperature profiles, view angles, surface pressure field, pixel locations, and QC flags. Data from each band/channel should be calibrated. Ancillary input data are dynamic and static (See section 3.3 for more details). Dynamic data includes: NCEP model temperature profile and surface pressure). Static input data is the set of ozone regression coefficients.

3.4.2.6 Configure angles, load predictors

In this section of the algorithm space pixels and bad pixels (based on QC flags) are skipped. For every pixel that remains the predictors are assembled. The cloud mask is not applied to allow the users to make decisions on how to apply the mask once the data is generated.

3.4.2.7 Test total column ozone against thresholds

Prior to output the ozone values are checked against maximum and minimum thresholds of 650 Dobson Units (DU) and 100 DU respectively. The thresholds are based on the product's required range of performance.

3.4.3 Algorithm Output

The ABI ozone algorithm provides a field of total column ozone that is stored in a NetCDF4 format output file. Under mode 3, the ozone algorithm has a 60 minute refresh, therefore it should be run once an hour. The ozone algorithm also has a 10 km horizontal resolution requirement. To meet this requirement, the pixel resolution ozone product with a quality flag of good (zero) will be averaged over a 5x5 pixel box. A summary of the output data sets is provided in Table 3.8.

Table 3.8 *Summary of ABI ozone code output data*

ABI ozone code output			
Name	Type	Description	Dimension
o3_col	End-product	Total column ozone (NetCDF4)	grid (xsize, ysize)
o3_pqi	Quality Assurance flags	Product quality flags for TCO. 0 for good TCO values, 1 for TCO less than 100 DU, 2 for TCO greater than 650 DU, 3 is for space pixels, 4 is for bad or missing input data.	grid (xsize, ysize)
Metadata	Output metadata	<ol style="list-style-type: none"> 1. Total column ozone statistical information: minimum, maximum, mean, and standard deviation 2. Number of Quality Assurance (QA) flag values 3. Definition of each QA flag value 4. Percent of retrievals with each QA flag value 5. Total number of retrieval pixels 	11 values, 5 strings

4. TEST DATASETS AND OUTPUTS

The development, implementation, and testing of the GOES_R ABI ozone detection algorithm is limited to proxy data sets from SEVIRI. Standard numerical weather prediction models do not handle ozone very well and typically insert climatology, which is of little benefit to an algorithm that relies on the coupling between ozone and thermal properties of the atmosphere.

4.1 Simulated Input Data Sets

SEVIRI data are used as proxy input data sets for the GOES-R ABI Ozone algorithm. SEVIRI bands are sufficiently similar to ABI that for this application they can be used (with their own regression coefficients). Both SEVIRI and ABI require NWP data to reach performance level of the GOES Sounder. Table 4.1 shows the bands used for ozone detection with the GOES Sounder, ABI, and SEVIRI. ABI has two bands that SEVIRI lacks. These bands would give a modest improvement to the ozone product.

SEVIRI data allows for 15 minute full disk images of a resolution comparable to ABI, SEVIRI pixels are nominally 9 km² versus 4 km² for ABI, so processing time on SEVIRI data needs to exceed specifications by a factor of 2.25,

The dataset used for algorithm testing during development consisted of Met-8 SEVIRI from August 2006; February 1-14, 2007; and April 1-10, 2007. This provides coverage over a range of seasons. The ozone product was produced at full instrument resolution without binning to 10 km resolution as specified in the requirements.

The delivered algorithm package includes the following SEVIRI cases:

- 1) August 24-25, 2006 (2 hours each day)
- 2) February 24-25, 2007 (2 hours each day)

Table 4.1 Bands used for ozone regression with different instruments

GOES-12			ABI			SEVIRI		
Band	NEDR	Wavelength (μm)	Band	NEDR	Wavelength (μm)	Band	NEDR	Wavelength (μm)
18	0.0009	3.75						
17	0.0022	3.98	1	-	0.47			
16	0.0024	4.12	2	-	0.64	1	-	0.635
15	0.0066	4.45	3	-	0.87	2	-	0.81
14	0.0062	4.53	4	-	1.38			
13	0.0062	4.57	5	-	1.61	3	-	1.64
12	0.11	6.5	6	-	2.25			
11	0.059	7.01	7	0.0038	3.9	4	0.0046	3.92
10	0.099	7.44	8	0.058	6.19	5	0.0098	6.2
9	0.14	9.72	9	0.0827	6.95			
8	0.11	10.96	10	0.0958	7.34	6	0.0226	7.35
7	0.11	11.99	11	0.1304	8.5	7	0.0948	8.7
6	0.14	12.66	12	0.1539	9.61	8	0.0975	9.66
5	0.34	13.34	13	0.1645	10.35			
4	0.39	13.63	14	0.1718	11.2	9	0.1247	10.8
3	0.45	14.03	15	0.1754	12.3	10	0.1923	12
2	0.61	14.38	16	0.5237	13.3	11	0.4178	13.4
1	0.77	14.66						

Figure 4.1 shows an example image from 23 UTC on 1 August 2006 which shows the entire hemisphere at SEVIRI's full 3 km resolution. Major ozone features are visible in the upper latitudes and over the North Atlantic. During the Northern Hemisphere's summer, total column ozone at high latitudes will not necessarily reach 400 DU, as seen in Figure 4.1. The high latitudes of the Southern Hemisphere, during its winter, are not included in the image.

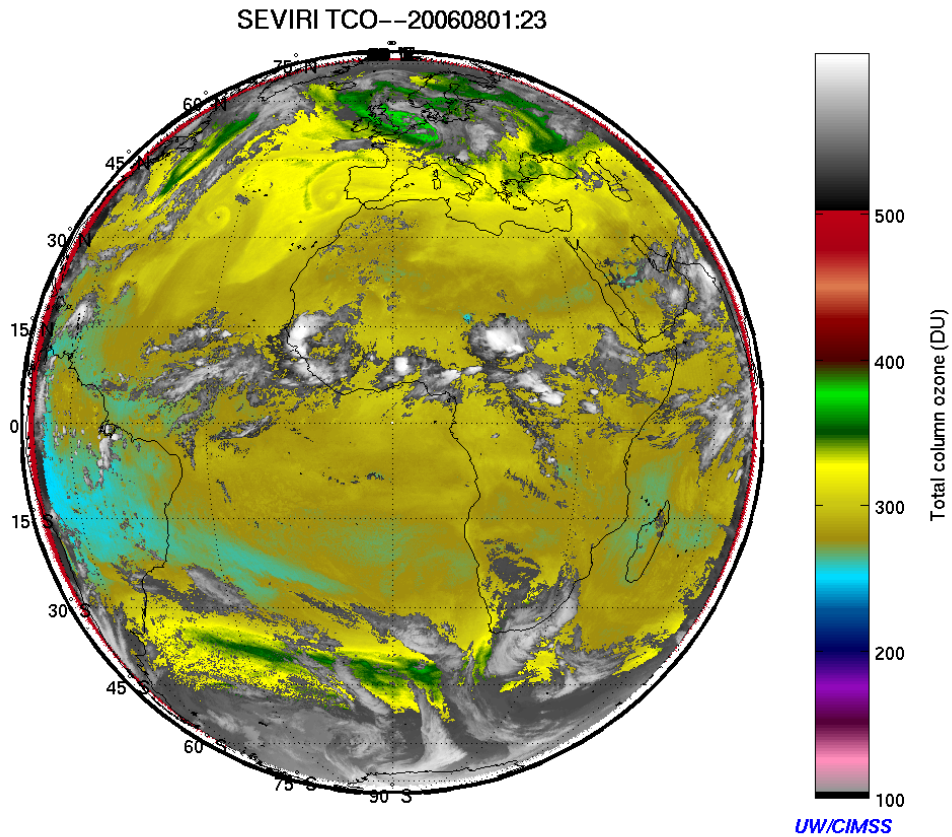


Figure 4.1 SEVIRI TCO data for 23 UTC on 1 August 2006. The red fringe is due to the visualization software.

The full day loop of this data shows the synoptic-scale ozone features moving. Ozone, due to its relationship to PV, effectively reflects the height of the tropopause, meaning ozone features generally change as fast as the synoptic weather. (Wimmers et al, 2003; Knox and Schmidt, 2004) Typically, ozone has been treated as a daily value, but the total column over one's head can change by as much as 50% in a matter of hours, with accompanying changes in the synoptic weather. The typical example is a strong cold front with a well-defined tropopause fold. ABI and instruments like it are not particularly sensitive to ozone in the boundary layer, where most ozone formation due to anthropogenic pollution occurs. Transport is the primary cause of ozone change over a particular earth location.

In some places, such as over northern Africa, a bias was introduced into the data due to a combination of surface characteristics and a relatively dry atmosphere. This impact is illustrated in Figure 4.2.

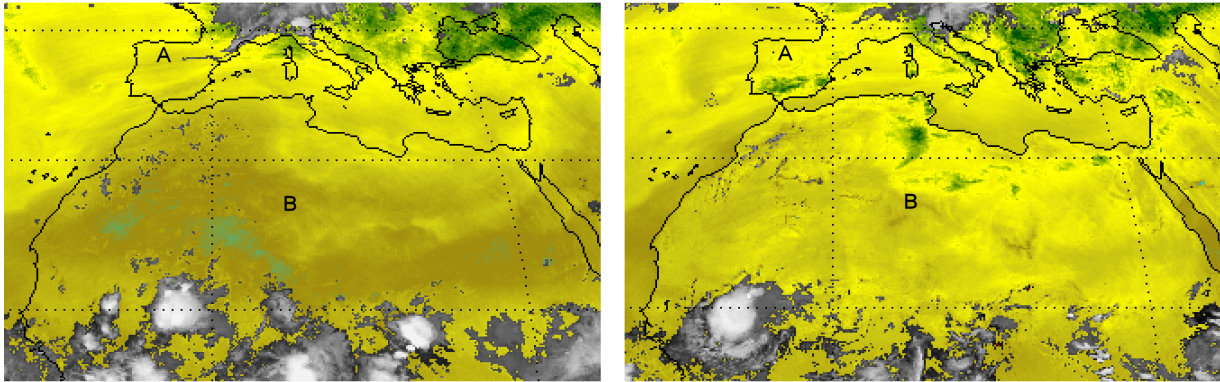


Figure 4.2 SEVIRI TCO at 1:00 UTC and 12:00 UTC on 1 August 2006. Left: 1:00 UTC 1 August 2006, Right: 12:00 UTC 1 August 2006.

The GOES I-M Sounder TCO experimental product often shows a diurnal variation over hot surfaces, and as expected this behavior is observed in SEVIRI TCO data as well. Label A shows how the hot, reflective surface of southern Spain effectively enhances a pre-existing streamer. Similar behavior is seen over the Sahara at label B. In both regions the total precipitable water is very low, allowing more surface signal to reach the satellite..

4.2 Output from Simulated Inputs Data Sets

Assessment of the ozone data's accuracy is accomplished by comparison with ozone data from the Ozone Mapping Instrument (OMI) on the Aura satellite. OMI is an ultraviolet sensor that follows on the tradition of the Total Ozone Mapping Spectrometer (TOMS) and has been validated against ground-based Dobson Photospectrometers and shown to be accurate to within 1%. (Veefkind et al, 2006)

The delivered algorithm package includes the following SEVIRI cases:

- 3) August 24-25, 2006 (2 hours each day)
- 4) February 24-25, 2007 (2 hours each day)

The results presented in this section assess performance of the algorithm over a longer time period.

4.2.1 Precision and Accuracy Estimates

For clear sky pixels, simulations show that the ozone product should achieve better than 25 DU precision and 15 DU accuracy within a local zenith angle of 65° for clear sky pixels. At greater local zenith angles, the accuracy and precision cannot be guaranteed to reach that threshold. This is due to the large footprint of the pixel, the long, slant-wise column, and the higher likelihood of undetected cloud contamination within the pixel.

Table 4.2 lists the precision and accuracy measures for all of the tested data. Pixels were screened for clouds (only clear sky pixels were accepted), all surface types and local zenith angles were included. The ozone algorithm exceeds the product requirements. Section 4.2.2 looks at precision and accuracy estimates for various scenarios.

The comparisons between Met-8 SEVIRI and OMI are produced by remapping OMI footprints to the SEVIRI projection and determining which Met-8 clear-sky pixels fit into each footprint. OMI footprints are 13 km by 24 km as satellite nadir, as opposed to Met-8 footprints which are 5 km by 5 km, tilted so as to appear diamond shaped, and spaced every 3 km. OMI footprints are determined by deriving footprint corners from the footprint centers and remapping those footprint polygons to the Met-8 SEVIRI fixed grid projection. From that point spatial co-location is a simple matter of looking at the two fixed grids and averaging together clear-sky SEVIRI ozone values within each OMI footprint.

Temporal co-location is very tight, SEVIRI values are within 15 minutes of OMI values thanks to SEVIRI's high refresh rate. This allows for a comparison of nearly instantaneous measurements.

Table 4.2 *Comparison of SEVIRI and OMI Validation to Requirements*

	Number of co-locations	Accuracy (DU) (req: 15 DU)	Precision (DU) (req: 25 DU)
August 2006; February 1-14 and April 1-10, 2007	5,796,726	3.3	14.8

Figures 4.3 and 4.4 show an example of the co-located pixels on 14-15 February 2007. Figure 4.3 is the Met-8 SEVIRI ozone values averaged into and plotted as OMI footprints. Figure 4.4 is the OMI data for the same cloud-free locations. Gaps are due to clouds and the space between OMI orbital passes. Time differences led to some discontinuities in ozone features. However, the overall ozone patterns are the same, with most gradients matching well between the two satellites. The most notable variation in the gradients occurs in South Africa, during their summer. The Met-8 ozone has a slight high ozone bias in part of that country. Section 4.2.2 examines the impact of hot surfaces and dry atmospheres on the Met-8 ozone product.

Met-8 SEVIRI TCO Remapped to OMI Footprints

14-15 February 2007

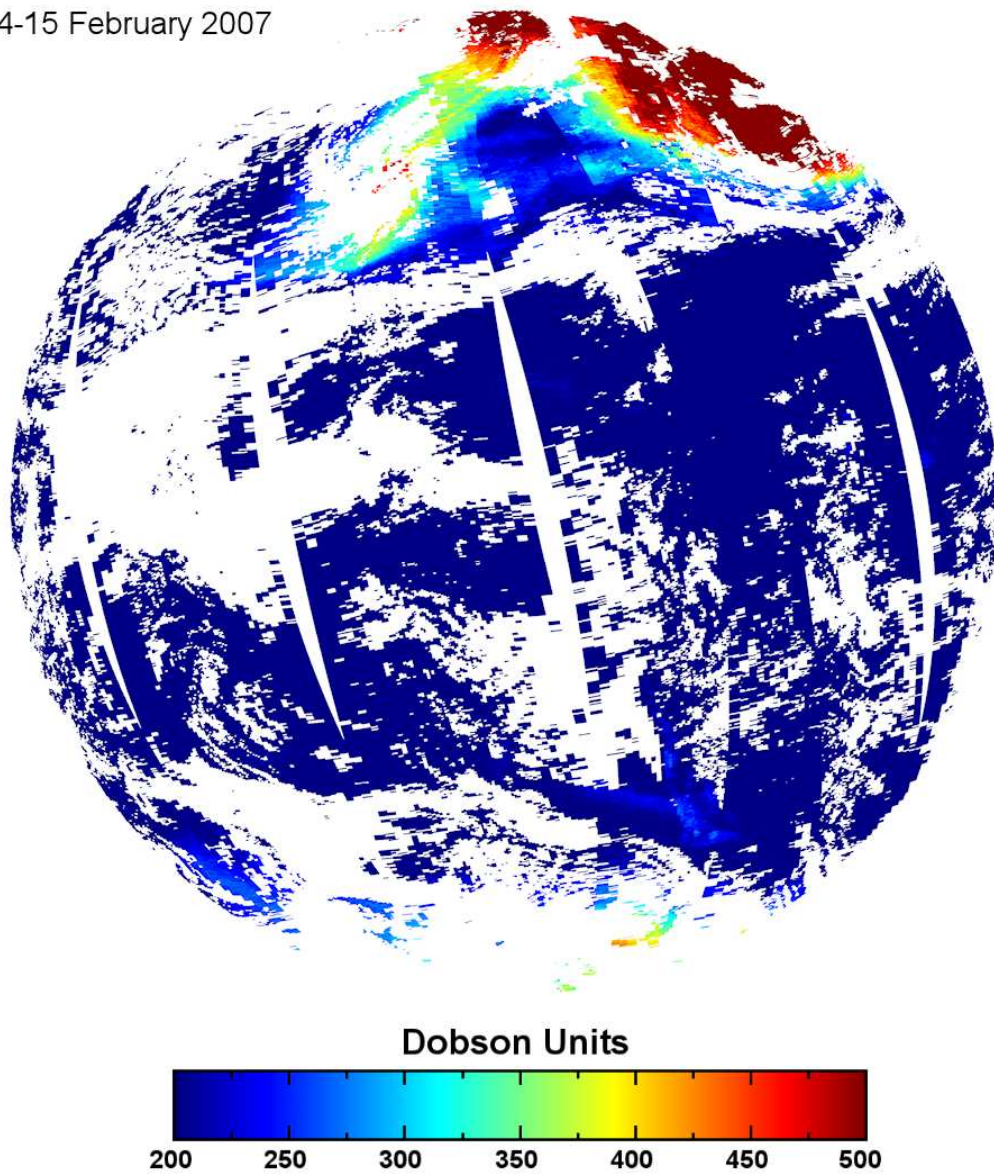


Figure 4.3 Met-8 SEVIRI total column ozone co-located in time and space with OMI total column ozone. Only SEVIRI clear-sky pixels were used.

OMI TCO Projected to OMI Footprints

14-15 February 2007

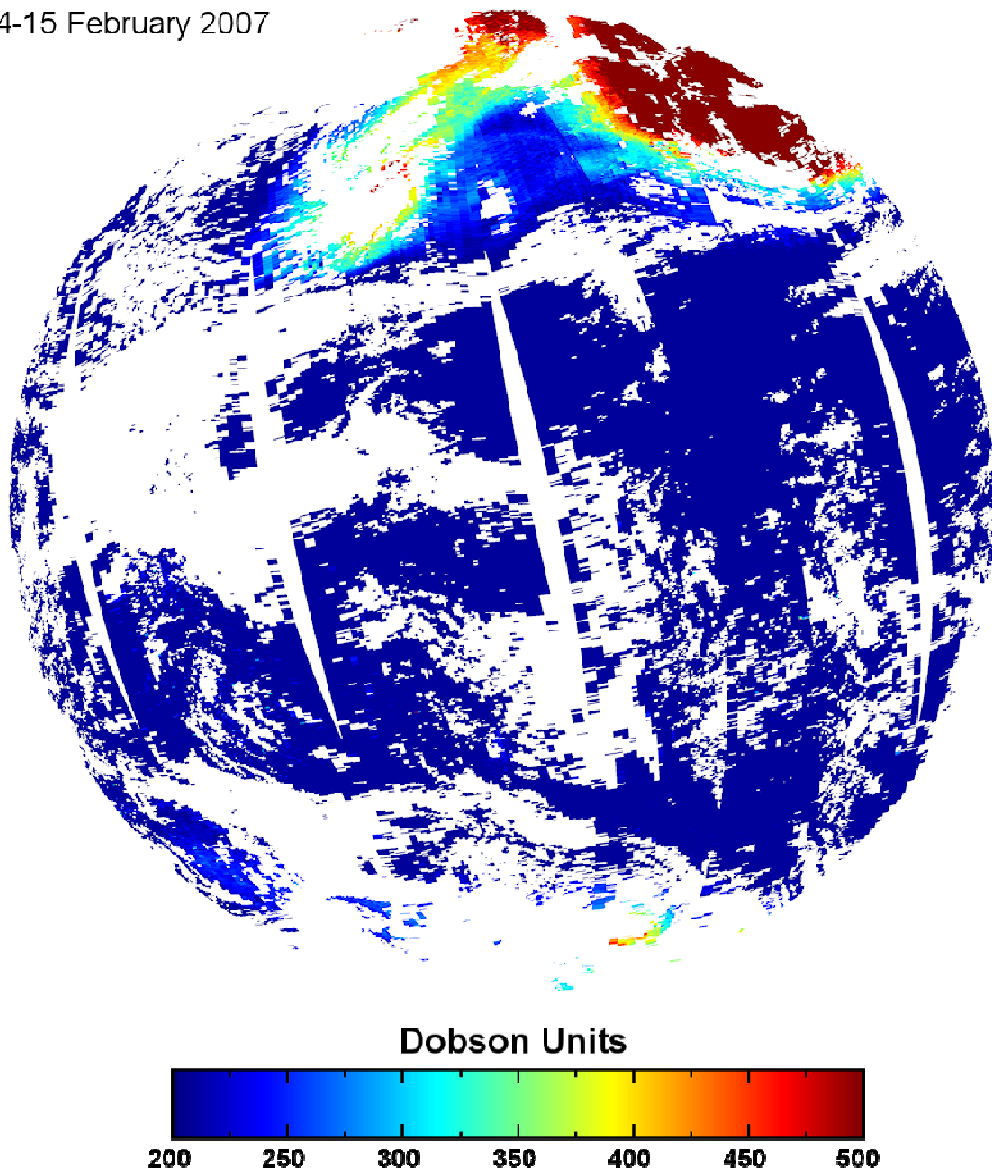


Figure 4.4 OMI total column ozone for 14-15 February 2007. Locations corresponding to SEVIRI clear-sky pixels were used.

4.2.2 Error Budget

The largest source of error for broadband infrared retrievals of total column ozone is from inadequate characterization of surface emissivity variations, allowing diurnal heating to exceed the range in the regression training dataset. The impact is particularly pronounced when the water vapor column is dry, though that is not the driving factor. Instrument noise is the next largest factor. For broadband instruments, increasing instrument noise by a factor of two generally increases %RMSE by $<0.5\%$ (typically about 1.5 DU), indicative of the efficiency of the ozone regression in extracting the useful information of the broadband data. For the same

instruments removing noise completely from simulations results in a minimal improvement of %RMSE, on the order of 0.8% (typically about 2.4 DU). For this reason averaging pixels to reduce noise has a small impact on %RMSE, precision, and accuracy. For other predictors (surface pressure, month, latitude, land fraction) errors of 20% have shown a minimal impact in previous studies. (Schmidt, 2000; Li et al, 2001; Li et al, 2007; Jin et al, 2008)

The definitions of accuracy and precision used herein were taken from the GOES-R ABI F&PS: **Product Measurement Accuracy (non-categorical products)** - Product Measurement Accuracy is defined for non-categorical products as the systematic difference or bias between the derived parameter and ground truth. It is determined by computing the absolute value of the average of differences between the derived parameter and ground truth over a statistically significant population of data such that the magnitude of the random error is negligible relative to the magnitude of the systematic error. (CCR01292, CCR01635)

Product Measurement Precision (non-categorical products) - Product measurement precision is the one-sigma standard deviation of the differences between the derived parameters and ground truth over the same population of data used to compute the product measurement accuracy. (CCR01292, CCR01635)

Table 4.3 lists the accuracy and precision for all pixels, land pixels excluding desert, desert pixels, and water pixels for all processed data and August 2006 alone. All pixels for April 2007 are also included. Only clear sky pixels were selected, and no local zenith angle threshold was used. The surface type determination was made using the land surface mask. Thanks to the large volume of SEVIRI data anywhere from 1,000,000 to 5,800,000 co-located pixels were available to provide statistics.

The table and following figures illustrate how diurnal surface temperature changes impact the ozone product, both over the full testing period and during August 2006 alone. Water surfaces have the least diurnal surface temperature variation and have the best accuracy and precision, whereas desert surfaces have the most diurnal temperature variation and worst accuracy and precision values. Performance over land, excluding desert, falls in between water and desert. Figures 4.2, 4.3, and 4.4 show two different examples of the effect of diurnal temperature variations, one over the Sahara in August and the other over dry parts of South Africa in February, dates well into summer in both regions.

While water has the best accuracy of the surface types, it too shows noticeable patterns within the scatter plot. Incomplete cloud masking, incorrect surface type determination, and systematic factors such as biases dependent upon latitude and viewing angle could account for those trends.

Table 4.3 Accuracy and Precision Results for Met-8 SEVIRI vs OMI Comparisons

	Number of co-locations	Accuracy (DU) (req: 15 DU)	Precision (DU) (req: 25 DU)	RMSE (DU)
August 2006; February 1-14 and April 1-10, 2007 (all clear-sky pixels)	5,796,726	3.3	14.8	15.1

August 2006; February 1-14 and April 1-10, 2007 (non-desert land)	1,862,589	3.3	14.4	14.7
August 2006; February 1-14 and April 1-10, 2007 (desert)	1,177,329	14.8	12.9	19.6
August 2006; February 1-14 and April 1-10, 2007 (water)	2,756,808	1.5	13.1	13.1
August 2006 (all clear-sky pixels)	3,408,432	6.5	13.3	15.8
August 2006 (desert only)	681,994	18.3	11.9	17.4
August 2006 (non-desert land)	1,124,385	6.5	12.5	14.1
August 2006 (water only)	1,602,053	1.4	11.1	11.2
April 2007 (all clear-sky pixels)	1,052,090	1.2	15.4	15.4

In all cases described above, the algorithm meets the F&PS requirements.

Figures 4.5-4.8 are scatter plots of the Met-8 ozone data versus the corresponding OMI data for the test data period August 2006, February 1-14 and April 1-10 2007. Figure 4.5 shows all of the data for the test period, followed by the scatter plot over all land but desert, desert, and water for Figures 4.6, 4.7, and 4.8 respectively. As indicated by the data in the table, desert pixels produce the worst results, as reflected in the scatter plot in Figure 4.7.

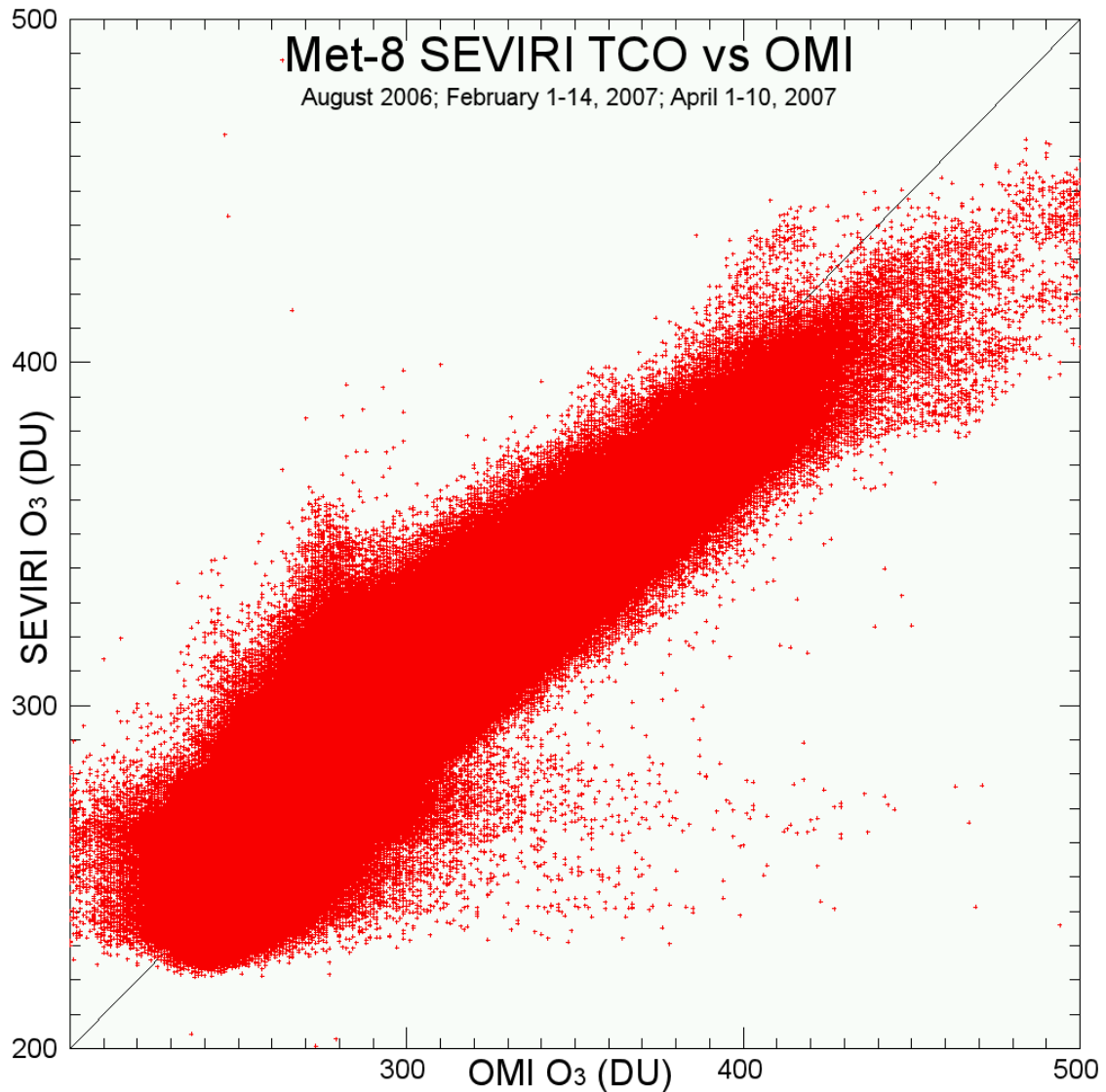


Figure 4.5. Met-8 SEVIRI vs OMI total column ozone for all cloud-free pixels during the test data period August 2006, February 1-14 and April 1-10 2007. Accuracy is 3.3 DU and precision is 14.8 DU.

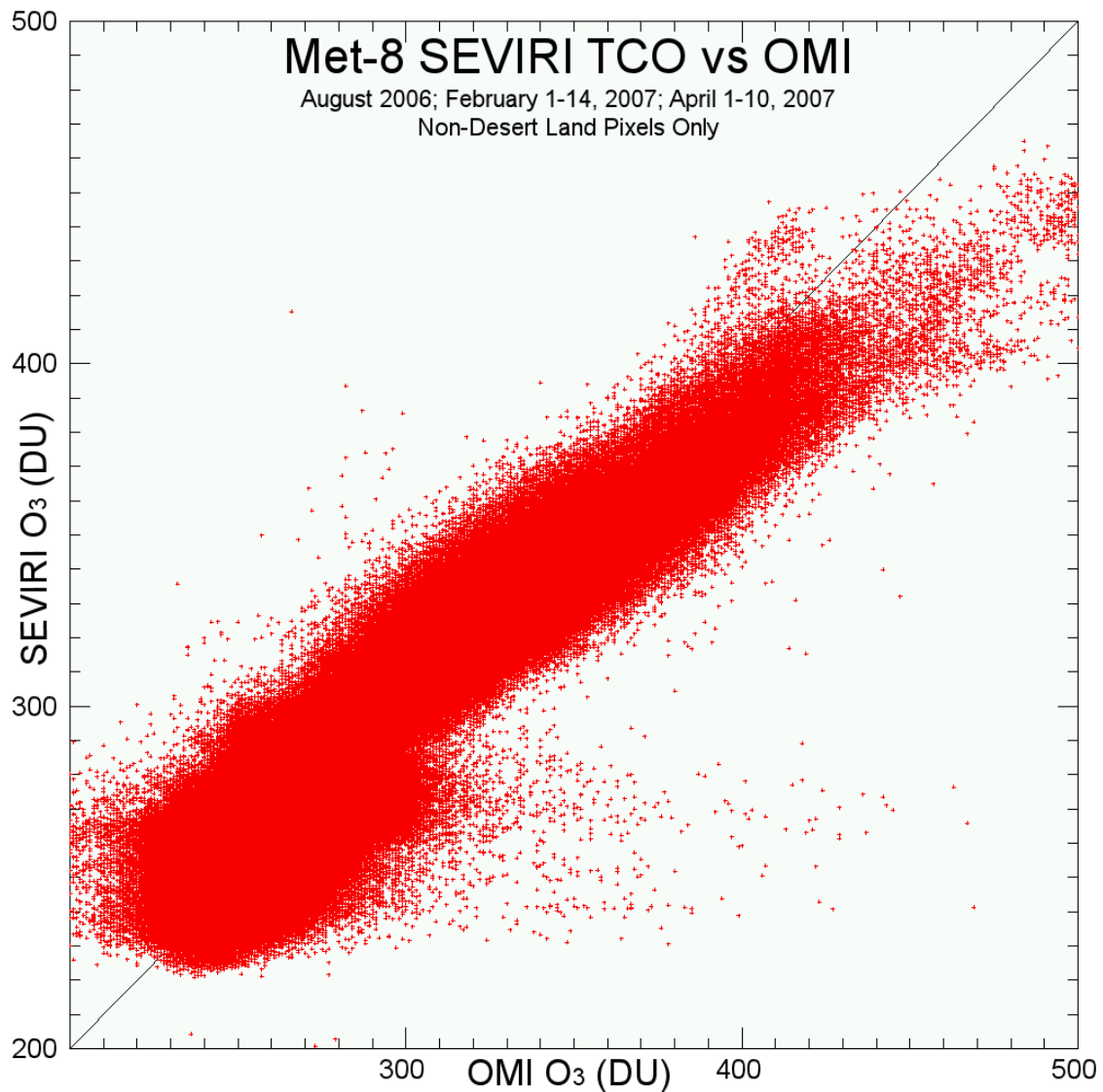


Figure 4.6. *Met-8 SEVIRI vs OMI total column ozone for all cloud-free, non-desert land pixels during the test data period August 2006, February 1-14 and April 1-10 2007. Accuracy is 3.3 DU and precision is 14.4 DU.*

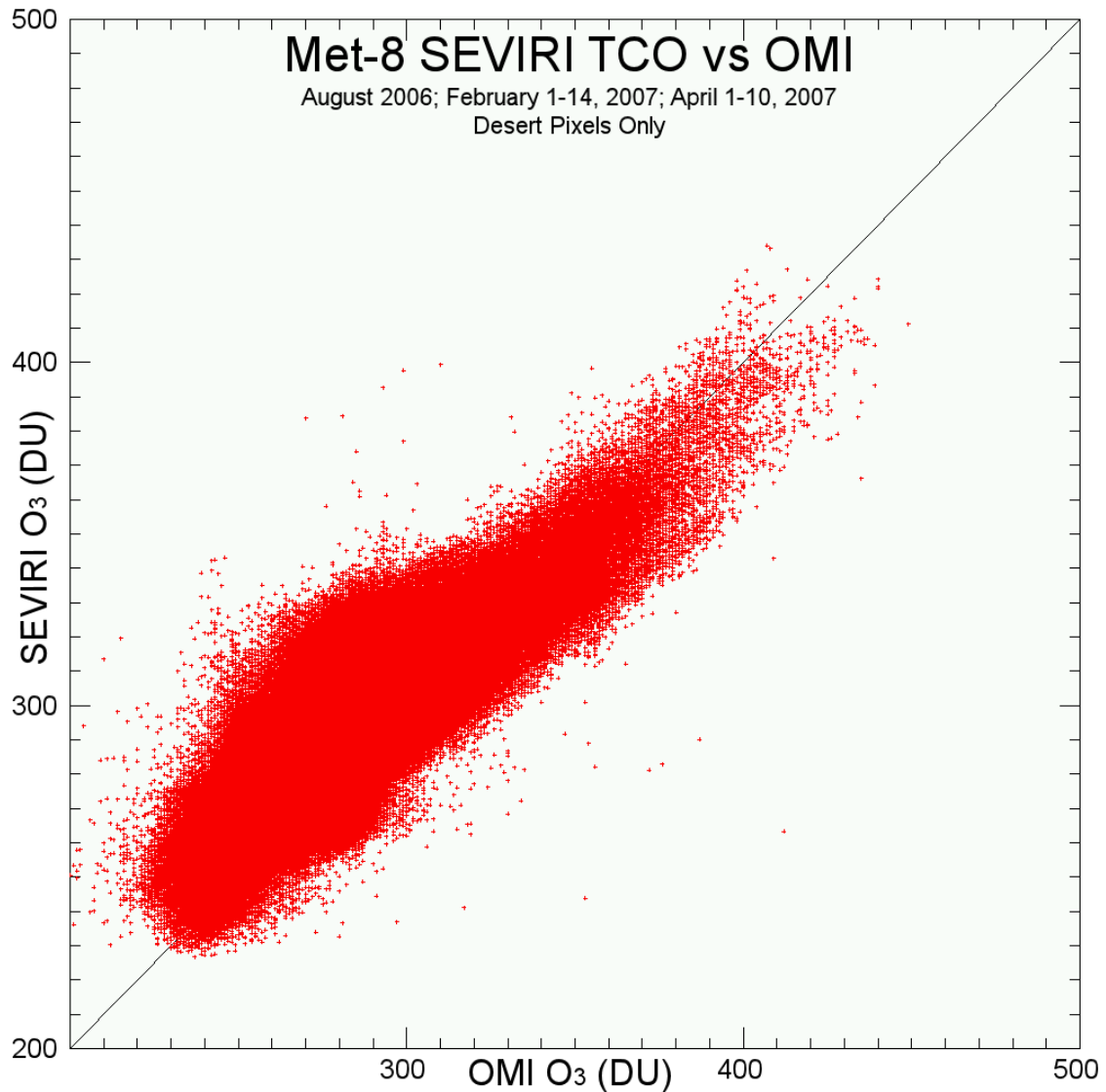


Figure 4.7. Met-8 SEVIRI vs OMI total column ozone for all cloud-free desert pixels during the test data period August 2006, February 1-14 and April 1-10 2007. The high ozone bias of Met-8 total column ozone over desert can be seen as the large region of points above the 1:1 line. Accuracy is 14.8 DU and precision is 12.9 DU.

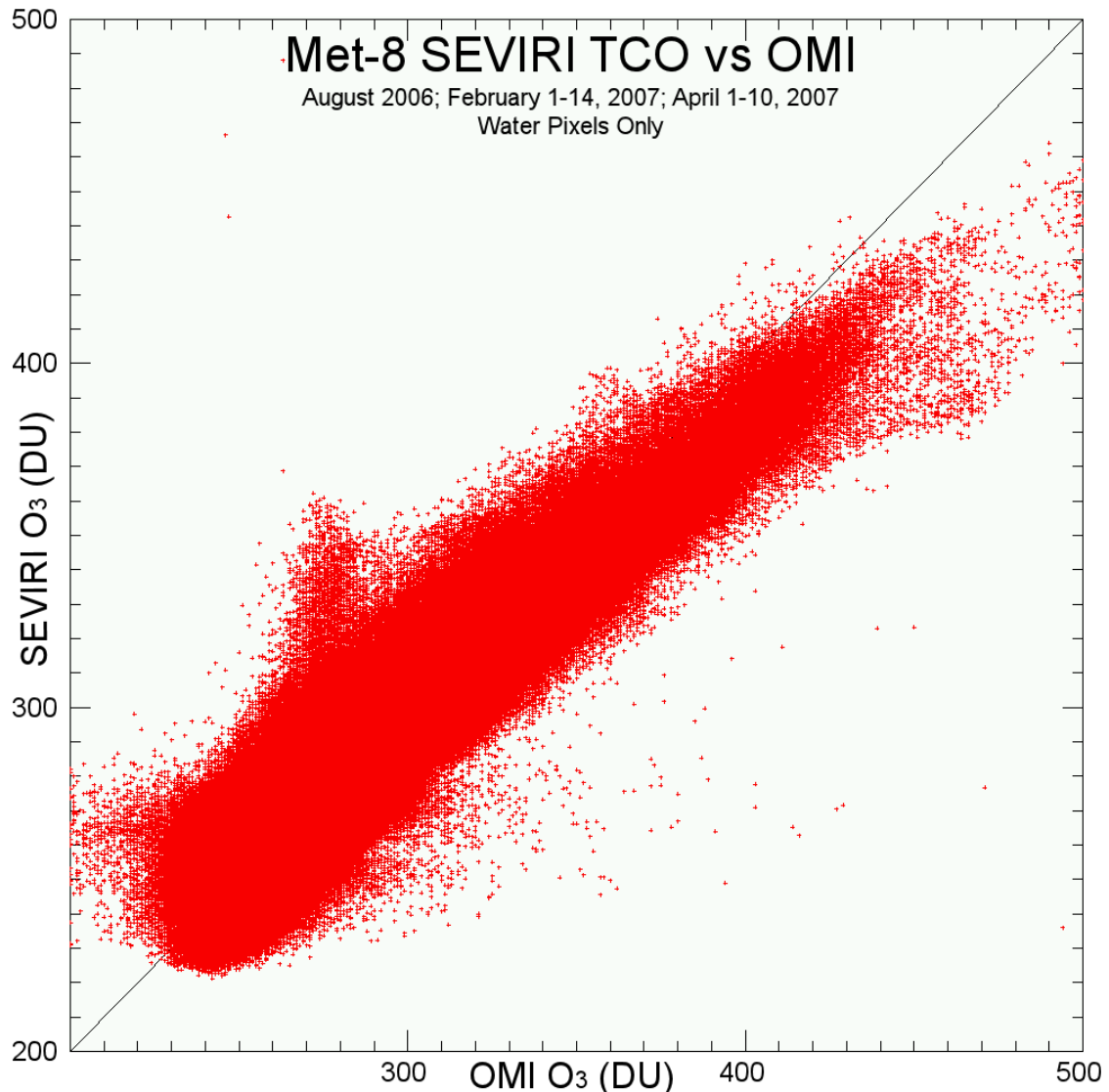


Figure 4.8. *Met-8 SEVIRI vs OMI total column ozone for all cloud-free pixels during the test data period August 2006, February 1-14 and April 1-10 2007. Accuracy is 1.5 DU and precision is 13.1 DU.*

Figure 4.5 shows all of the data for the test period, followed by the scatter plot over all land but desert, desert, and water for Figures 4.6, 4.7, and 4.8 respectively. As indicated by the data in the table, desert pixels produce the worst results, as reflected in the scatter plot in Figure 4.7.

5. PRACTICAL CONSIDERATIONS

The ozone algorithm is relatively stable computationally as it does not involve iterations on data values but rather a straightforward vector and matrix multiplication.

5.1 Numerical Computation Considerations

The primary numerical operation is a dot product of a matrix and a vector. That operation results in the natural logarithm of the total column ozone value. This makes the algorithm quite stable numerically but also exposes sensitivity to correlations between the input predictors, which is tied to the difficulty that models have with generating useful proxy data for the ozone algorithm.

While numerically stable overall, undoing the natural logarithm does to a small extent enhance the impact of small variations in precision between machines and compilers. Testing has showing such impacts to be less than 0.0001% of a total column ozone value, however.

5.2 Programming and Procedural Considerations

The ozone algorithm needs access to the set of regression coefficients read from a file. Otherwise the algorithm is very straightforward. Regression coefficients should not change unless substantial changes to the instrument (central wavelength of bands, NEDT) occur.

5.3 Quality Assessment and Diagnostics

The ozone product should be screened against the ABI cloud mask once it is produced. Ozone is calculated for all valid pixels, but it is left to the user of the data to determine which values to use.

The ozone algorithm was designed this way to account for anticipated future upgrades that could allow for calculation of ozone over some clouds. Routine and automated (to the maximum extent possible) validation based on comparison to OMI (and follow-on polar orbiting UV-based ozone detection missions) is the most effective way to assess the ABI ozone product. Daily visualization for imagery coincident with OMI (or its successors) provides a quick-look qualitative assessment of algorithm performance. Quantitative comparisons can be made through generation and evaluation of statistics summarizing ongoing intercomparisons of ABI ozone and OMI (or its successors). Monthly statistics, including %RMSE and relative bias (accuracy and precision), should also be generated.

5.4 Exception Handling

Most run-time exceptions are handled by the system running the ozone algorithm. The ozone code fails and does not run if the regression coefficients cannot be found. The ozone code fails for a given pixel if **any** of the required inputs are missing. In that case the algorithm proceeds to the next pixel.

The quality flag for a valid ozone value is 0 or undefined. If the ozone value is less than or equal to 100 DU, the flag is 1. For ozone values greater than or equal to 650 DU, the flag is 2. Space pixels have a flag of 3. Missing input data results in a flag of 4.

5.5 Algorithm Validation

Future validations include processing ozone in real-time and having automatic OMI co-locations and statistics generated. This allows for additional improvements and refinements to help reduce issues such as the false diurnal ozone variations over desert.

Proxy ABI data generated from models data that do handle ozone are becoming available, and once it is that will be used with the TCO product made with ABI regression coefficients. In the GOES-R era, validation will involve comparison to ozone from UV satellite instruments, comparison to Dobson-Brewer photospectrometers, and available sondes. The latter two are effectively measurements of opportunity (clear sky is required). OMI is well characterized with regards to these instruments and given larger OMI data volume it will remain the primary source of validation.

6. ASSUMPTIONS AND LIMITATIONS

6.1 Performance

The ABI ozone algorithm performance assumptions are as follows. The algorithm has been tested on Pentium III Xeon and Intel Core 2 Duo class CPUs and meets the latency requirement on those platforms. The code is written and compiled as a single-threaded application, and substantial enhancements are possible if multi-threading and other advanced features of modern CPUs are applied. Overall performance is proportional to the number of pixels processed. Performing operations on data in memory with a minimum number of disk accesses is the best way to maintain performance.

Other performance assumptions include: sub-pixel cloud contamination is minimized (the ABI cloud mask does its job), remapping to a perfect navigated grid does not have a discernable impact on the ozone product, and surface emissivity variations can adversely impact ozone (specifically over deserts, as seen over the Sahara in the examples presented herein).

Regression is predicated on training with a known set of inputs. Replacement of bad input values with 0 can be attempted, but by design this algorithm is not designed to function on anything less than the full set of input data.

6.2 Assumed Sensor Performance

The ABI sensor data is assumed to be within specifications. Radiances are treated as is with no adjustments for remapping. The L1B remapping of ABI data should have no discernable impact on the ozone product.

Errors in input radiances can have an impact on the algorithm, especially when the errors are in the 9.6 μm band. That band has the largest contribution to the ozone product. Radiance errors outside of specification in other bands will not impact the ozone product as strongly.

6.3 Pre-Planned Product Improvement

The ozone algorithm has two pre-planned improvements which are under consideration.

6.3.1 Increased number of training profiles

The group of training profiles used to create the ozone regression coefficients covers a wide range of weather conditions, but since the profiles are only available from certain sites and at certain times, additional profiles can improve the quality of the regression. This type of improvement has been made to the GOES Sounder Ozone algorithm on a recurring basis for the last several years as new collocated profiles have become available from various sources.

6.3.2 Ozone over low clouds

Low, relatively warm cloud tops emit strongly enough in the long-wave infrared to make ozone estimation possible. This improvement will require an additional set of regression coefficients and modifications to the processing in the algorithm, but the changes are relatively minor to the software. This improvement is being researched.

6.3.3 Missing inputs

The current ozone algorithm is unable to function properly if inputs are missing – regression with one set of coefficients does not allow for it. To allow for graceful degradation scenarios where acceptable performance can be achieved without certain inputs will be examined. Not all scenarios can be realistically accounted for, but cases such as missing temperature profiles or the loss of certain bands can be addressed.

7. REFERENCES

- Aminou, D., et. al., 2003: Meteosat Second Generation: A comparison of on-ground and on-flight imaging and radiometric performances of SEVIRI on MSG-1. Proceedings of The 2003 EUMETSAT Meteorological Satellite Conference, Weimar, Germany, 29 September 3 October 2003, 236243.
- Bowman, K. P., A. J. Krueger, 1985: A global climatology of total ozone from the Nimbus-7 total ozone mapping spectrometer. *J. Geophys. Res.*, 90, 79677976.
- Burrows, J. P., et. al. 1999: The Global Ozone Monitoring Experiment (GOME): Mission concept and first scientific results. *J. Atmos. Sci.*, 56(2), 151175.
- Divakarla, M. G., C. D. Barnet, M. D. Goldberg, L. M. McMillin, E. Maddy, W. Wolf, L. Zhou, X. Liu, 2006: Validation of Atmospheric Infrared Sounder temperature and water vapor retrievals with matched radiosonde measurements and forecasts. *J. Geophys. Res.*, 111(D09). doi:10.1029/2005JD006116.

- Engelen, R. J., G. L. Stephens, 1997: Infrared radiative transfer in the 9.6- μ m band: Application to TIROS operational vertical sounder ozone retrieval. *J. Geophys. Res.*, 102, 6929-6939.
- Eyre, J. R., H. M. Woolf, 1988: Transmittance of atmospheric gases in the microwave region: A fast model. *Appl. Opt.*, 27(15), 3244-3249.
- Hannon, S., L. L. Strow, W. W. McMillan, 1996: Atmospheric infrared fast transmittance models: A comparison of two approaches. *Proc. Conf. on Optical Spectroscopic Techniques and Instrumentation for Atmospheric and Space Research II*, Denver, CO, SPIE, vol. 2830, 94105.
- Heath, D. F., A. J. Krueger, H. A. Roeder, and B. D. Henderson, 1975: The solar backscatter ultraviolet and total ozone mapping spectrometer (SBUV/TOMS) for NIMBUS G. *Opt. Eng.*, 14, 3233-31.
- Jin, X., J. Li, C. C. Schmidt, T. J. Schmit, J. Li, 2008: Retrieval of Total Column Ozone From Imagers Onboard Geostationary Satellites. *IEEE Transactions on Geoscience and Remote Sensing*, 46(2), 479-488.
- Knox, J. A., C. C. Schmidt, 2004: Using GOES total column ozone to diagnose stratospheric intrusions and nowcast non-convective cyclone windstorms: methodology and initial results. *Proceeding of 13th Conference on Satellite Meteorology and Oceanography*, 20-23 September, 2004. American Meteorological Society, Boston, MA.
- Levelt, P. F., E. Hilsenrath, G. W. Leppelmeier, G. H. J. van den Oord, P. K. Bhartia, J. Tamminen, J. F. de Haan, and J. P. Veefkind, 2006: Science objectives for the Ozone Monitoring Instrument. *IEEE Trans. Geosci. Remote Sensing*, 44(5), 1199-1208. doi:10.1109/TGRS.2006.872336.
- Li, J., C. C. Schmidt, J. P. Nelson, T. J. Schmit, and W. P. Menzel, 2001: Estimation of total atmospheric ozone from GOES sounder radiances with high temporal resolution. *J. Atmos. Oceanic Technol.*, 18(2), 157-168.
- Li, J., Jun Li, C. C. Schmidt, J. P. Nelson III, T. J. Schmit, 2007: High temporal resolution GOES Sounder single field of view ozone improvements. *Geophys. Res. Lett.*, 34, L01804. doi:10.1029/2006GL028172.
- Neuendorffer, A. C., 1996: Ozone monitoring with TIROS-N operational vertical sounders. *J. Geophys. Res.*, 101(D13), 18807-18828.
- Rothman, L. S., et. al., 1998: The HITRAN molecular spectroscopic database and HAWKS (HITRAN Atmospheric Workstation). *J. Quant. Spectrosc. Radiat. Transfer*, 60(5), 665-710.
- Schmetz, J., P. Pili, S. Tjemkes, D. Just, J. Kerkmann, et al, 2002: An Introduction to Meteosat Second Generation (MSG). *Bull. Amer. Meteor. Soc.*, 83(7), 977-992.

- Schmidt, C. C., 2000: Hourly ozone estimation utilizing GOES I-M sounder. M.S. thesis, Department of Atmospheric and Oceanic Sciences, University of WisconsinMadison. [Available from Schwerdtfeger Library, 1225 W. Dayton St., Madison, WI 53706]
- Schmit, T. J., M. M. Gunshor, W. P. Menzel, J. J. Gurka, J. Li, A. S. Bachmeier, 2005: Introducing the next-generation Advanced Baseline Imager on GOES-R. *Bull. Amer. Meteor. Soc.*, 86(8), 1079-1096.
- Schoeberl, M. R., A. R. Douglass, E. Hilsenrath, P. K. Bhartia, R. Beer, J. W. Waters, M. Gunson, L. Froidevaux, J. Gille, J. Barnett, P. F. Levelt and P. DeCola, 2006: Overview of the EOS Aura mission. *IEEE Trans. Geosci.Remote Sensing*, 44(5), 1066-1074. doi:10.1109/TGRS.2005.861950.
- Seemann, S., E. Borbas, B. Knuteson, G. Stephenson, A. Huang, 2007: A global infrared surface emissivity database for clear sky atmospheric regression, Submitted to *J. Appl. Meteorol.*, (submitted).
- Seemann, S., J. Li, W. P. Menzel, and L. Gumley, 2003: Operational Retrieval of Atmospheric Temperature, Moisture, and Ozone from MODIS Infrared Radiances. *J. Appl. Meteorol.*, 42(8), 1072-1091.
- Smith, W. L., H. M. Woolf, C. M. Hayden, D. C. Wark, L. M. McMillin, 1979: The TIROS-N operational vertical sounder. *Bull. Amer. Meteor. Soc.*, 60(10), 1177-1187.
- Strabala, F. I., S. A. Ackerman, W. P. Menzel, 1994: Cloud properties inferred from 8-12 micron data. *J. App. Meteor.*, 33(2), 212-229.
- Veefkind, J. P., J. F. de Haan, E. J. Brinksma, M. Kroon and P. F. Levelt, 2006: Total Ozone from the Ozone Monitoring Instrument (OMI) Using the DOAS technique. *IEEE Trans. Geo. Rem. Sens.*, 44(5), 1239-1244. doi:10.1109/TGRS.2006.871204.
- Wimmers, A. J., J. L. Moody, E. V. Browell, J. W. Hair, C. F. Butler, W. B. Grant, M. A. Fenn, C. C. Schmidt, J. Li, B. A. Ridley, 2003: Signatures of tropopause folding in satellite imagery. *J. Geophys Res.*, 108(D4), 8360. doi:10.1029/2001JD001358.

Appendix 1: Common Ancillary Data Sets

1. LAND_MASK_NASA_1KM

a. Data description

Description: Global 1km land/water used for MODIS collection 5

Filename: lw_geo_2001001_v03m.nc

Origin: Created by SSEC/CIMSS based on NASA MODIS collection 5

Size: 890 MB.

Static/Dynamic: Static

b. Interpolation description

The closest point is used for each satellite pixel:

- 1) Given ancillary grid of large size than satellite grid
- 2) In Latitude / Longitude space, use the ancillary data closest to the satellite pixel.

2. NWP_GFS

a. Data description

Description: NCEP GFS model data in grib format – 1 x 1 degree (360x181), 26 levels

Filename: gfs.tHHz.pgrbfhh

Where,

HH – Forecast time in hour: 00, 06, 12, 18

hh – Previous hours used to make forecast: 00, 03, 06, 09

Origin: NCEP

Size: 26MB

Static/Dynamic: Dynamic

b. Interpolation description

There are three interpolations are installed:

NWP forecast interpolation from different forecast time:

Load two NWP grib files which are for two different forecast time and interpolate to the satellite time using linear interpolation with time difference.

Suppose:

T1, T2 are NWP forecast time, T is satellite observation time, and $T1 < T < T2$. Y is any NWP field. Then field Y at satellite observation time T is:

$$Y(T) = Y(T1) * W(T1) + Y(T2) * W(T2)$$

Where W is weight and

$$W(T1) = 1 - (T-T1) / (T2-T1)$$

$$W(T2) = (T-T1) / (T2-T1)$$

NWP forecast spatial interpolation from NWP forecast grid points. This interpolation generates the NWP forecast for the satellite pixel from the NWP forecast grid dataset.

The closest point is used for each satellite pixel:

- 1) Given NWP forecast grid of large size than satellite grid
- 2) In Latitude / Longitude space, use the ancillary data closest to the satellite pixel.

NWP forecast profile vertical interpolation

Interpolate NWP GFS profile from 26 pressure levels to 101 pressure levels

For vertical profile interpolation, linear interpolation with Log pressure is used:

Suppose:

y is temperature or water vapor at 26 levels, and y101 is temperature or water vapor at 101 levels. p is any pressure level between p(i) and p(i-1), with $p(i-1) < p < p(i)$. y(i) and y(i-1) are y at pressure level p(i) and p(i-1). Then y101 at pressure p level is:

$$y_{101}(p) = y(i-1) + \log(p[i] / p[i-1]) * (y[i] - y[i-1]) / \log (p[i] / p[i-1])$$